78

Egypt. J. Chem. **Vol. 65,** No. SI:13B pp. 815-826 (2022)

Egyptian Journal of Chemistry

Polymer/Inorganic Hybrid Layer Enhancing Photoactivity of TiO₂NWs for The Removal of Dyes and Quantum Dots Solar Cells

Hossam E. M. AbdelMoneim, [a] Magdy A. Wassel, [a] Samar H. Bendary, [b] Ahmed S. Elfeky,[a] Sawsan A. Mahmoud [b*]

[a] Chemistry Department, Faculty of Science, Al-Azhar University, Cairo, Egypt.
[b] Egyptian Petroleum Research Institute, 1-Ahmed El-Zomr St., P.O. Box 11727, Nasr City, Cairo, Egypt

Abstract

A polymer solution containing 0.5 wt.% polydiallyl dimethyl ammonium chloride was used to modify graphitic carbon nitride by the sol-carbonization method (PDDA $_{(0.5)}$ @ g-C$_3$N$_4$). Titanium dioxide nanoparticles were synthesized by microwave irradiation followed by hydrothermal treatment to obtain titanium nanowires (TiNWs). The TiO$_2$NWs/ (PDDA $_{(0.5)}$ @g-C$_3$N$_4$) nanocomposite was prepared with different wt. % of TiO$_2$NWs to (PDDA $_{(0.5)}$ @g-C$_3$N$_4$), 50:50, and 30:70 by the wet impregnation method. The prepared nanocomposites were applied in twin applications: photo-catalysis and quantum dot solar cells. Basic blue (Bb) and Methyl Orange (MO) were used as pollutants, and the degradation efficiencies were 96, 94, 90.8, 63.7, and 30.7% for TiO$_2$NWs/ (PDDA $_{(0.5)}$ @g-C$_3$N$_4$) (50:50), TiO$_2$NWs/ (PDDA $_{(0.5)}$ @g-C$_3$N$_4$) (30:70), TiO$_2$NWs, g-C$_3$N$_4$, and (PDDA $_{(0.5)}$ @ g-C$_3$N$_4$), respectively, compared with the control experiment (without catalyst) at 14.8%. A perceived improvement in photovoltaic performance of TiO$_2$NWs/ (PDDA $_{(0.5)}$ @g-C$_3$N$_4$) (50:50) was observed. A conversion efficiency of 2.8% with a V_{oC} of 504 mV, J_{SC} of 9.92 mA cm^{-2}, and a fill factor (FF) of 0.58 was achieved using 7 layers of CdS QD by the SILAR method.

Keywords:nanocomposite; conductive polymer; cationic dye; photo-degradation; (QDSSCs); (SILAR).

1. Introduction

g-C$_3$N$_4$ is a bright conjugated semiconductor polymer that is used in solar power and environmental treatment transformations as a metal-free photocatalyst sensitive to visible light [1,2]. The estimated bandgap of g-C$_3$N$_4$ is 2.7 eV, which extremely enhances the response to the visible light range [3-5]. Unfortunately, the qualification of bulk g-C$_3$N$_4$ as a photo-active material is unsatisfactory due to its rapid rate of recombination, low quantum performance, incomplete absorption of sunlight, and low surface area [6, 7]. Conjugation with high conductivity materials (graphene, carbon nanotubes) [8, 9], nanoporous structure modification [9, 10], metals or nonmetal doping [11, 12], supramolecular self-assembly [13], and hetero-junction construction [14, 15] have all been addressed in the development of g-C$_3$N$_4$ photocatalytic activity. Combining g-C$_3$N$_4$ with other semiconductors can improve its ability to harvest visible light by promoting photo-generated charge separation and broadening the absorption spectrum [16-18]. Several studies have shown the effective construction of TiO$_2$/g-C$_3$N$_4$ hetero-structures composites with developed photo-catalytic activity for degradation of dye [19, 20], splitting of water [21], reduction of CO$_2$ [22], and photo-catalytic inactivation of bacteria [23] based on the matching of energy band structures. The construction of a TiO$_2$/g-C$_3$N$_4$ hetero-structure can reduce the recombination rate of produced electron-hole couples and even improve light absorption activity effectively [24]. It is well known that TiO$_2$ is a greatly considered photo-catalyst due to its features involving high photo-corrosion impedance, chemical inertness, low cost, and non-toxic material. However, when TiO$_2$ is used as an individual semiconductor, it has poor performance due to narrow photo-rejoinder and electron transportation becoming limited, and consequently, its performance decreases greatly. Lately, there have been successful approaches to developing the activities of TiO$_2$ through the construction of composite materials [25-30]. Recently, 1D-TiO$_2$ nanostructures involving TiO$_2$ nanowires [31], TiO$_2$ nanobelts [32, 33] have attracted the interest of researchers. X. Pan et al. [34] compare the degradation performance of GO/TiO$_2$ nanoparticles and GO/TiO$_2$ nanowires and show that GO/TiO$_2$ NWs are more uniformly dispersed on GO with less agglomeration than GO/TiO$_2$ NPs. Moreover, the crossed TiO$_2$ NWs act as a separate layer between graphene nanosheets and thus prevent restacking graphene layers, thereby increasing the

stability and photocatalytic activity of the composite catalyst. Sang et al. [32] reported the combination of the TiO_2 Nano-belts and GO. It was found that TiO_2 Nano-belts can encourage the transport of electrons effectively along the pivotal route, which is helpful for the separation of the carrier in the photo-catalytic process. It has been proposed that combining TiO_2 with other visible-light catalysts is a successful strategy. Among these visible-light catalysts are CdS [35, 36], $BiVO_4$ [37], and $g-C_3N_4$ [38]. Polymer/inorganic hybrid nanomaterial can be used in different applications, among which are catalysis, optics, and optoelectronics. However, the polymer composition usually has functions regarding their structure and may modify the mechanical features and final materials remediation. On the other hand, the inorganic ingredient can provide functions such as catalytic and optical activities of the polymer. The final characteristics of the hybrid nanomaterial are the combination of the independent ingredients with the unique outcome of synergistic effects [39]. Poly (diallyl dimethyl ammonium chloride) (PDDA) is an efficient ionic polymer characterized by its electronic properties in addition to its polyelectrolyte non-toxic properties. It was used in paper production systems for water treatment, mining, and biological areas (Chen et al., 2006), which were reported to be effectively functionalized graphene sheets noncovalently [39]. Furthermore, because it is non-hazardous, PDDA can be used as a reducing agent [40] with GO to replace other hazardous reducing agent materials. In addition, the metal oxide can be stabilized firmly during the deposition process by PDDA [41] with GO to replace other hazardous reducing agent materials. Herein, the authors interested in the synthesis and use of a ternary composite of $TiO_2NWs/$ (PDDA$_{(0.5)}$ @g-C_3N_4) (50:50) as an active photocatalyst to UV-Vis light and investigate its degradation efficiency toward cationic (Bb) and anionic (MO) dyes as organic pollutant models. Furthermore, the $TiO_2NWs/$ (PDDA$_{(0.5)}$ @g-C_3N_4) (50:50) composite was used as a photoelectrode to develop QDSSCs. As indicated to our insight, this is the first time using a PDDA to produce composite catalysts based on g-C_3N_4.

2. Material and methods

2.1. Materials;

All the used chemicals were analytical grade without refinement. Titanium (IV) isopropoxide (TTIP) and glacial acetic acid were obtained by Pan Reac Co., Spain. Sigma-Aldrich, Germany, supplied urea, absolute ethanol 99.8%, sodium chloride 99.0%, barium sulphate 99.99%, and PDDA, Mw = 1000–20000 g/mole, 20wt.% aqueous solution. Bb and MO dyes were purchased from Pub Chem.

2.2. Methods

2.3. Synthesis of TiO_2

According to the literature, TiO_2 was produced utilizing the microwave technique. [42]. The steps in this technique were to add 8 mL of TIP dropwise to 15.5 mL of glacial acetic acid while stirring vigorously, and then add 170 mL of deionized water dropwise to the mixture while swirling vigorously. The solution was agitated for 1 h to obtain a clear, clean solution. Finally, the solution was exposed to microwave electromagnetic radiation (LG Co., 2.45 GHz, 850w) for 6 min. The resulting white gel was filtered, rinsed with deionized water, and dried for several hours in the oven. The powder was then calcined for 5 h at 500ºC.

2.4. TiO_2 NWs Synthesis

10 g of TiO_2 was added to 10 M NaOH and agitated until a uniform dispersion was achieved. After that, the solution was loaded into a 400 mL Teflon-lined stainless-steel autoclave and placed in a preheated furnace at 170 °C for 20 h. The reaction was allowed to cool to room temperature naturally. The white precipitate was filtered, then washed three times with deionized water, acidified with 0.1M HCl to set the pH to roughly 7, and finally dried overnight at 40 °C [43].

2.5. Graphitic carbon nitride (g-C_3N_4) synthesis.

The following procedure was used to prepare g-C_3N_4 by thermal breakdown of urea: 10 g of CH_4N_2O was placed in a semi-covered crucible under ambient pressure in the air. The urea was dried at 80 ºC before being heated to 550 ºC in a muffle furnace for 3 h to complete the reaction. To eliminate any residual alkaline species (e.g. ammonia) adsorbed on the sample surface, the product was washed with nitric acid (0.1 mol L^{-1}) and distilled water, then dried at 80 ºC for 24 h [44].

2.6. Synthesis of PDDA @ g-C_3N_4

A simple sol-carbonization process was used to make PDDA@g-C_3N_4. g-C_3N_4 was dipped into 100 mL of PDDA solutions of varied weight percentages (0.1, 0.5, and 1.0) containing 0.1M NaCl and stirred continuously for 1 h at room temperature. The infiltrating PDDA@g-C_3N_4 was centrifuged to remove excess PDDA before drying at 105 ºC to yield PDDA modified g-C_3N_4 (PDDA$_{(x)}$ @ g-C_3N_4), where (x) refers to PDDA solution concentration [45].

2.7. Wet impregnation method for synthesis of $TiO_2NWs/PDDA_{(x)}$ @ g-C_3N_4 nanocomposite

The $TiO_2NWs/(PDDA_{(x)}@g-C_3N_4)$ nanocomposites were created by dissolving a calculated weight of PDDA$_{(x)}$@ g-C_3N_4 in ethanol and then adding TiO_2NWs to the resulting solution. After 30 minutes of stirring, the solvent evaporated. The $TiO_2NWs/(PDDA_{(x)}$ @ g-C_3N_4) nanocomposite was impregnated and dried at room temperature for 24 h before being annealed for 1 h at 400°C.

2.8. Fabrication of the QD photoanode layer

Homogeneous films of TiO₂NWs, TiO₂NWs/(PDDA$_{(0.5)}$ @ g-C₃N₄) (50:50), and TiO₂NWs/(PDDA$_{(0.5)}$ @ g-C₃N₄) (30:70) were coated via the doctor blade technique on cleaned ITO glass (ultrasonically cleaned in a mixture of distilled water, ethanol, and isopropanol in ratios of 1:1:1), and then different photo-electrodes TiO₂NWs/(PDDA$_{(0.5)}$ @ g-C₃N₄) (50:50) and TiO₂NWs/(PDDA$_{(0.5)}$ @ g-C₃N₄) (30:70) were prepared and sensitized with CdS QDs by the SILAR method. To deposit CdS QDs, TiO₂NWs, TiO₂NWs/(PDDA$_{(0.5)}$ @ g-C₃N₄) (50:50), and TiO₂NWs/(PDDA$_{(0.5)}$ @ g-C₃N₄) (30:70) films were first immersed in 0.1 M cadmium nitrate Cd(NO₃)₂ ethanol solution for 2 min as a Cd^{2+} source, then rinsed in ethanol to remove excess ions. The films were dipped into a 0.1 M Na₂S methanol solution for another 2 min to allow S^{2-} to react with the pre-adsorbed Cd^{2+} to form CdS. The tightly conjoined S^{2-} ions were eliminated by washing the film in methanol and then the films were dried at 60 ºC for 1 min. The whole procedure is called "one cycle," and the combined amount of CdS can be thickened periodically by the fabricated cycles.

2.9. Instrumentations and characterizations

The morphological analysis of TiO₂ anatase, TiO₂-NWs, TiO₂NWs/ (PDDA $_{(0.5)}$ @ g-C₃N₄) (50:50), and TiO₂NWs/(PDDA$_{(0.5)}$@g-C₃N₄)(30:70) composites was done by scanning-electron microscope (SEM) and energy-dispersive X-ray spectroscopy (EDS) by (Jeol JSM- 6510 LV).

Infrared analysis (FT-IR) was performed by a Nicolet Is-10 FT-IR spectrophotometer (Attenuated Total Reflection) mode from 4000 to 400 cm^{-1}.

X-ray diffraction spectroscopy was carried out using X PERT PRO-PAN Analytical.

High-Resolution transmission electron microscopy (HRTEM) was performed on JEOL (GEM-1230) at an operating voltage of 120 kV.

XPS was collected on K-ALPHA (Thermo Fisher Scientific, USA) with monochromatic X-ray Al K-alpha radiation -10 to 1350 e v spot size of 400 μm pressure 10-9 mbar full-spectrum pass energy of 200 e v and narrow-spectrum pass energy of 50 ev. Data was analyzed with Multi-Pak software and Casa-XPS processing.

The concentrations of Bb and MO dyes were detected using a Hach-UV/vis spectrophotometer (DR-6000).

Absorbance measurements of the prepared samples were recorded in the range of 200–1000 nm using a Hach-UV/vis spectrophotometer (DR-6000), allowing the band gap and absorbance calculation for the prepared materials. The samples were prepared to be suspended in a barium sulphate solution.

2.10. Dual-functional nanocomposite
2.10.1. Experiments with photodegradation

Bb and MO dye (**Fig.1**) were used to examine the photocatalytic activity of TiO₂-NWs, g-C₃N₄, PDDA$_{(0.5)}$@g-C₃N₄, and TiO₂NWs/(PDDA$_{(0.5)}$ @ g-C₃N₄) nanocomposites. A known concentration of Bb dye and the known weight of the prepared photocatalysts were exposed to UV-Vis light (UVA lamp, 15W, 368nm, Sylvania, Germany) for up to 120 min. Bb samples (about 5 ml) were taken out at interval times, centrifuged for 5 min at 800 RPM, and their absorbance was recorded at the maximum peak wavelength of 664 nm using a UV-Vis spectrophotometer (Model DR 6000, HACH). Different variables such as PDDA concentration, dye concentration (5, 10, and 20 ppm), and different nanocomposite weights (0.5, 1, and 2 g/L) that influence the photodegradation process were studied by UV-visible spectroscopy.
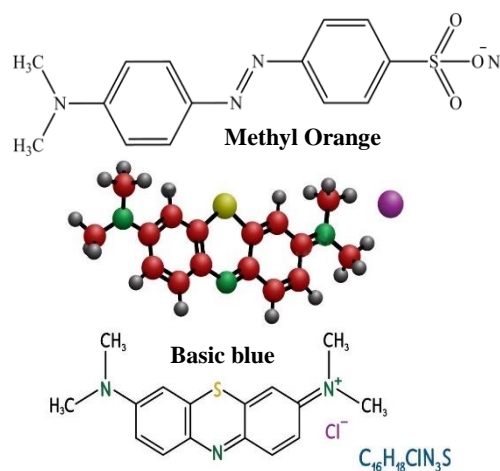

Fig.1. Molecular structure of Methyl Orange and Basic blue

2.10.2. QDSSCs:

After preparing the QD photoanode, homogeneous thin films of g-C₃N₄ nanocomposites were prepared and coated on the cleaned ITO glass as a photocathode. Working electrodes of as-prepared TiO₂NWs, TiO₂NWs/(PDDA$_{(0.5)}$ @ g-C₃N₄) (50:50), and TiO₂NWs/(PDDA$_{(0.5)}$ @ g-C₃N₄) (30:70) and g-C₃N₄ nanocomposite CEs were assembled as a double-decker-type cell, and a polysulfide electrolyte (2 M Na₂S, 2 M sulfur, and the active area of the cell was adjusted to be 4.25 cm². The fabricated cells were kept in the dark for 24 h and measurements were recorded for 1- 4 days to obtain the highest Voc values under sunlight illumination. The conversion efficiency of the solar cell (CE) can be calculated using the following equation:

$$CE = (J_{SC} \times V_{OC} \times FF) / P_{in}$$

Where J_{SC} is the short circuit photocurrent density, V_{OC} is the open-circuit voltage, FF is the fill factor

and P_{in} is the power intensity of the incident light. *FF* Values can be calculated from the current density-voltage (J-V) curves.

3. Results and discussion

3.1. *XRD and FTIR analysis of Nano-structure*

The crystal phase of g-C_3N_4, TiO_2, TiO_2NWs, $PDDA_{(0.5)}$ @ g-C_3N_4, and $TiO_2NWs/(PDDA_{(0.5)}$ @ g-C_3N_4) nanocomposites was identified by XRD and the results are shown in **Fig. 2A**. XRD shows diffraction peaks at 2θ angles of 25.64° (101), 37.82° (004), 48.33° (200), 54.19° (105), 55.02° (211), 62.81° (204), 68.94° (116), 69.73° (220), and 75.60° (215). The pattern could be assigned to a tetragonal anatase phase of TiO_2 according to JCPDS No. 21–1272. The XRD pattern of g-C_3N_4 shows the common peaks at 13.0° (100) and 27.5° (002) matched due to the inter-planer packing structure according to JCPDS Card No. 87-1526 [46]. The reduction in the hydrogen content through the release of ammonia leads to an increase in the crystallinity of g-C_3N_4. This indicates an increase in the number of stacked melon sheets per crystallite and a reduction in the stacking distance. This also indicates the decreasing distance between the sheets due to the decreasing distance of the nitrogen atoms. The XRD pattern of $PDDA_{(0.5)}$@g-C_3N_4, on the other hand, shows regular peaks like g-C_3N_4 but with less intensity at angles of 13.0° and 27.5°. This can be attributed to the increase in the inner nitrogen distances, which results in the distortion of the molen sheets and, consequently, the partial distortion of the 2-dimensional arrangement. This indicates the heterojunction of the polymer in the g-C_3N_4 structure [47]. The $TiO_2NWs/(PDDA_{(0.5)}$ @ g-C_3N_4)nanocomposites samples show the presence of g-C_3N_4 and TiO_2NWs diffraction peaks, indicating the coexistence of g-C_3N_4 and TiO_2. However, with increasing the TiO_2NWs content, the intensity of this peak decreases obviously.
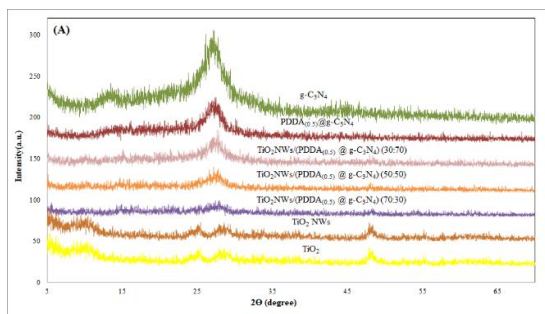

Fig.2A. XRD of g-C_3N_4, TiO_2, TiO_2NWs, $PDDA_{(0.5)}$ @ g-C_3N_4, and $TiO_2NWs/(PDDA_{(0.5)}$ @ g-C_3N_4) nanocomposites

The FTIR spectra of pure TiO_2NWs, g-C_3N_4, $PDDA_{(0.5)}$@g-C_3N_4, and $TiO_2NWs/(PDDA_{(0.5)}$ @ g-C_3N_4) nanocomposite samples are shown in Fig. 2B. The absorption band at 1603 cm^{-1} is attributed to the C–N stretching vibration modes, whereas the four strong absorption bands centred at 1259, 1343, 1400, and 1556 cm^{-1} are attributed to the C–N heterocycle stretching mode [48], and the absorption band at 803 cm^{-1} is attributed to the out-of-plane ring bending modes of C–N heterocycles [49]. Furthermore, the band at 700 cm^{-1} can be assigned to the TiO_2 characteristic peak [50], while the broad bands from 3000 to 3600 cm^{-1} can be assigned to the TiO_2 OH group stretching vibrations and g-C_3N_4 terminal secondary amide RCONHR′ group stretching vibrations [51], indicating the presence of g-C_3N_4 and TiO_2 in composites.
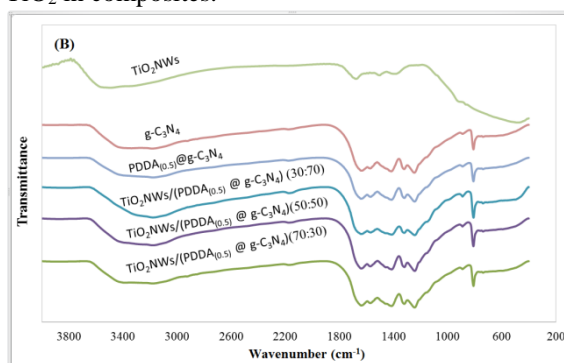

Fig.2B. FTIR spectra of TiO_2NWs, g-C_3N_4, $PDDA_{(0.5)}$ @ g-C_3N_4, and $TiO_2NWs/(PDDA_{(0.5)}$ @ g-C_3N_4) nanocomposites.

3.2. TEM, SEM, and EDS analysis

TEM, SEM, and EDS mapping analysis were used to investigate the morphological properties of TiO_2NWs, g-C_3N_4, and $TiO_2NWs/(PDDA_{(0.5)}$ @ g-C_3N_4) nanocomposite in **Fig. 3. (A, D),** the synthesized TiO_2NWs are agglomerated and unevenly crisscrossed with an average diameter of 8-15 nm and a length of 42-80 mm. The variety in the length of nanowires is due to the fracture of the nanowires during material preparation. **Fig. 3 (B, E)** g-C_3N_4 exhibits a two-dimensional (2D) structure with a rugged surface and porous structures. To improve the poor charge transport, TiO_2NWs were rationally incorporated with $PDDA_{(0.5)}$ @ g-C_3N_4 to form a nanocomposite $TiO_2NWs/(PDDA_{(0.5)}$ @ g-C_3N_4) as illustrated in **Fig.3 (C, F).** TiO_2NWs are well dispersed on the surface and sandwiched in between $PDDA_{(0.5)}$ @g-C_3N_4. Thus, TiO_2NWs can act as skeletons between $PDDA_{(0.5)}$ and g-C_3N_4 nanosheets. The EDS signals indicate the presence of C, N, O, Na, and Ti with a wt. % of 8.73, 7.35, 31.83, 9.71, and 41.14, respectively (**Fig.3 G**). The mapping of the relevant elements, including C, N, O, and Ti, indicated that TiO_2NWs were well dispersed on the surface of $PDDA_{(0.5)}$ @ g-C_3N_4 (**Fig.3 H**).
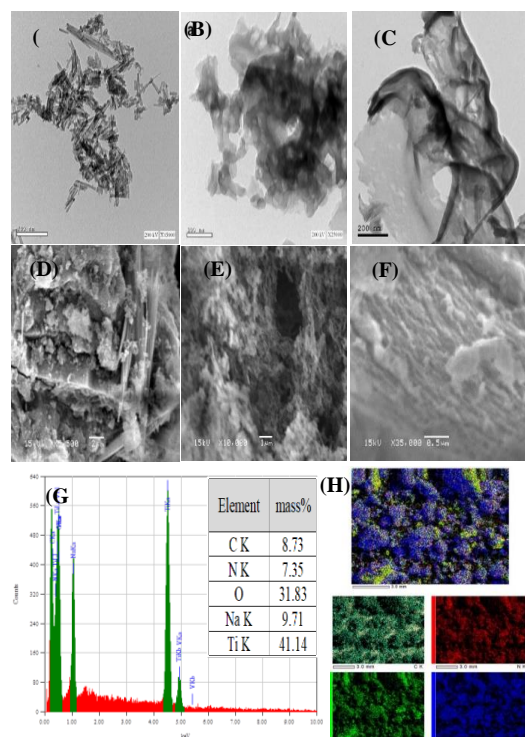
Fig.3. TEM, SEM and EDS mapping analysis of TiO$_2$NWs, g-C$_3$N$_4$, and TiO$_2$NWs/(PDDA$_{(0.5)}$ @ g-C$_3$N$_4$) nanocomposite.

3.3. XPS examination

XPS was measured to obtain information about the chemical states and composition of the TiO$_2$NWs/(PDDA$_{(0.5)}$@g-C$_3$N$_4$)(50:50) composite surface. The survey of the TiO$_2$NWs/(PDDA $_{(0.5)}$ @g-C$_3$N$_4$) (50:50) spectrum in **Fig. 4A** shows the presence of Ti 2p, O 1s, C 1s, and N 1s signals in the nanocomposite. **Fig. 4B** shows the C 1s spectrum of the TiO$_2$NWs/(PDDA$_{(0.5)}$@g-C$_3$N$_4$)(50:50) composite with three main deconvolution components at 284.5, 286.42 and 287.81 eV. The lower bonding energy peak (284.5 eV) suggests the presence of (sp^2) N-C=N (sp^2), whereas the next peak at 286.42 eV corresponds to C (-N) 3.0. The third peak of C1s at 287.81 eV is evidently assigned to carboxylate carbon (O-C=O) [52, 53]. As shown in **Fig. 4C**, the N 1s spectrum of the TiO$_2$NWs/(PDDA $_{(0.5)}$ @g-C$_3$N$_4$) (50:50) nanocomposite was deconvoluted into four peaks. The Ti-N bond was assigned the peak at 398.34 eV, while N-(C)^3 was assigned the peak at 399.8 eV [54].The other peak at 400.61 eV is convenient with sp^2 hybridized C=N bonds in pyridine (C$_2$H$_5$N), and the last peak at 403.8 eV can be attributed to (-NH$_2$). The O 1s spectrum of TiO$_2$NWs/(PDDA $_{(0.5)}$@g-C$_3$N$_4$) (50:50) composite can be deconvoluted into peaks at (529.9 and 531.8 eV) which are assigned to (Ti-O bond and O-H bond, respectively) [55]. As shown in **Fig. 4D** The O 1s peak at 534.9 eV suggested the presence of PDDA

$_{(0.5)}$@g-C$_3$N$_4$ and TiO$_2$NWs due to the coexistence of the two components in heterojunction. Further, the position of peaks shifted left slightly suggests that TiO$_2$NWs chemically bind to PDDA $_{(0.5)}$@g-C$_3$N$_4$ rather than physical binding [56]. **Fig. 4E** shows the Ti 2p$_{3/2}$ and 2p$_{1/2}$ spin-orbit coupling peaks at 458.2 and 471.1 eV, respectively, which are assigned to Ti-O in the TiO$_2$NWs. The deconvolution of the Ti region of the TiO$_2$NWs/(PDDA $_{(0.5)}$@g-C$_3$N$_4$) (50:50) nanocomposite implies the presence of Ti-N or/and Ti-C (at 458.25 and 460.89 eV for Ti 2p$_{3/2}$ and at 463.72 and 465.28 for 2p$_{1/2}$, respectively). It can be concluded that there is a chemical bond between the Ti and C and/or N of the PDDA $_{(0.5)}$@g-C$_3$N$_4$ [57].
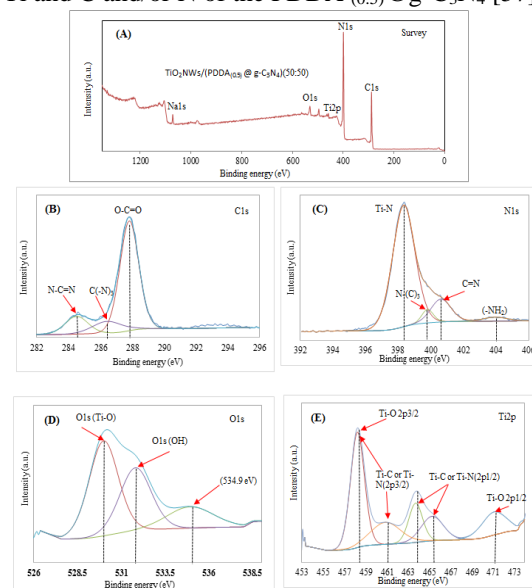

Fig.4. XPS spectrum of TiO$_2$NWs/(PDDA$_{(0.5)}$ @ g-C$_3$N$_4$) (50:50) nanocomposite.

3.4. Optical properties

Fig.5 shows the UV-Vis adsorption spectra of TiO$_2$NWs, TiO$_2$NWs/(PDDA $_{(0.5)}$@g-C$_3$N$_4$)(50:50), g-C$_3$N$_4$, and PDDA $_{(0.5)}$@g-C$_3$N$_4$. According to the formula $\lambda = 1240/Eg$, the band gap energy of the TiO$_2$NWs, TiO$_2$NWs/PDDA $_{(0.5)}$ @g-C$_3$N$_4$ (50:50), g-C$_3$N$_4$ and PDDA $_{(0.5)}$ @g-C$_3$N$_4$ are 3.3, 2.75, 2.8, and 2.64 eV, respectively. TiO$_2$ could absorb ultraviolet light with a wavelength below 400 nm due to its intrinsic band gap of anatase TiO$_2$NWs while the absorption edge of the TiO$_2$NWs/PDDA $_{(0.5)}$ @g-C$_3$N$_4$ (50:50) shifted towards the visible region at 450 nm. The findings of the band gap show that the implementation of PDDA $_{(0.5)}$ @ g-C$_3$N$_4$ decreases the band gap energy of TiO$_2$. These results confirm that the UV-Vis light absorption of TiO$_2$ nanowires has been effectively enhanced by the impregnation of PDDA $_{(0.5)}$ @g-C$_3$N$_4$ nanoparticles, which is beneficial for developing the photo-catalytic activity of TiO$_2$ [58].

Calculations of the Valence Band (Ev) and the Conduction Band Edge (Ec)

According to the UV-Vis adsorption spectra, the band gap energies of TiO$_2$NWs, TiO$_2$NWs/(PDDA$_{(0.5)}$@g-C$_3$N$_4$) (50:50), g-C$_3$N$_4$, and PDDA$_{(0.5)}$@g-C$_3$N$_4$ are 3.3, 2.75, 2.8, and 2.64 eV, respectively. The following equations were used to calculate the (VB), (CB) edge [59]:

$$EVB = \chi - Ee + 1/2\, Eg \qquad (1)$$
$$ECB = EVB - Eg \qquad (2)$$

Where E$_{VB}$ and E$_{CB}$ are the edge potentials of the valence and conduction bands, respectively, χ is the electronegativity of the semiconductor, which is the geometric mean of the electronegativity of the constituent atoms [60]. TiO$_2$-NWs and g-C$_3$N$_4$ have calculated values of 5.81 eV and 4.67 eV, respectively [60]. Ee is the energy of free electrons on the hydrogen e scale (4.5 eV) and is the band gap energy of the semiconductor. Based on band gap Eg positions, the band edge potentials of VB and CB for TiO$_2$-NWs are 2.96 eV and - 0.34 eV, while for g-C$_3$N$_4$ they are 1.57 eV and -1.23 eV.
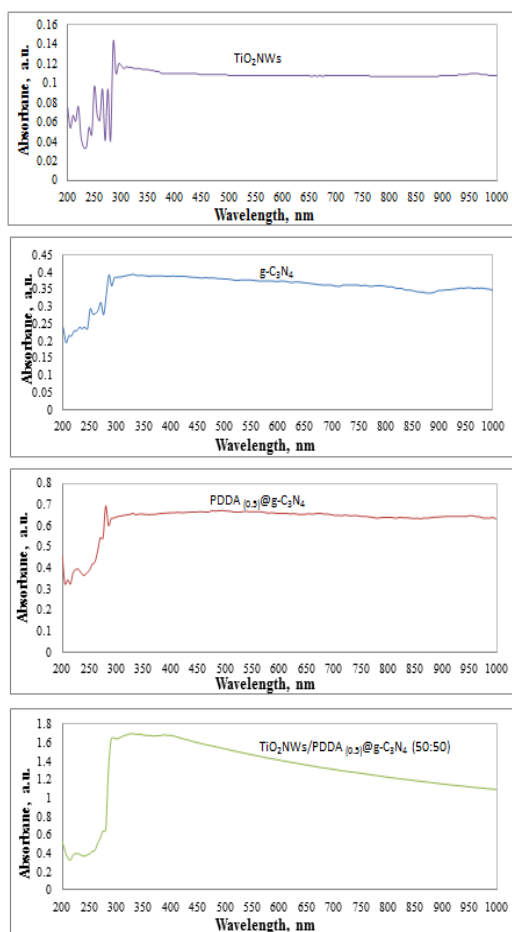

Fig.5. UV-Vis adsorption spectra of TiO$_2$NWs, g-C$_3$N$_4$, PDDA$_{(0.5)}$@g-C$_3$N$_4$, and TiO$_2$NWs/(PDDA$_{(0.5)}$@g-C$_3$N$_4$)(50:50)

3.5. Photo-catalytic and adsorption properties

To assess photodegradation performance, one of the most common pollutant models was used, and a 10 mg/L aqueous solution of basic blue was exposed to UV-Vis light. Before irradiation, the solution was stirred for about 30 min to achieve an adsorption/desorption equilibrium between the dyes and the surface of the photocatalyst.

3.5.1. The effect of three (g-C$_3$N$_4$, PDDA, and TiO$_2$NWs) components on Basic blue degradation

Firstly, the three components will be examined individually and then together to discover the viability of enhancing the catalytic performance. As shown in **Fig. 7A**. When compared to the control (without catalyst), the photodegradation percentages were 96, 90.8, 63.7, and 30.7% for samples with TiO$_2$NWs/(PDDA$_{(0.5)}$@g-C$_3$N$_4$) nanocomposite as a more efficient catalyst, and TiO$_2$NWs, g-C$_3$N$_4$, and PDDA$_{(0.5)}$@g-C$_3$N$_4$, respectively. In addition, the photocatalytic performance of PDDA$_{(0.5)}$@g-C$_3$N$_4$ was found to be less than other components due to repulsion between the positive charge of PDDA as a cationic polyelectrolyte and Bb as a cationic dye (**Fig. 6**). During the irradiation process, electrons originating from the PDDA and g-C$_3$N$_4$ transfer to the CB of TiO$_2$NWs to participate in the redox reactions [61].
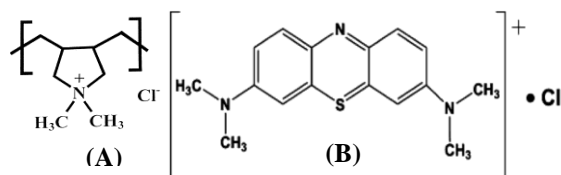

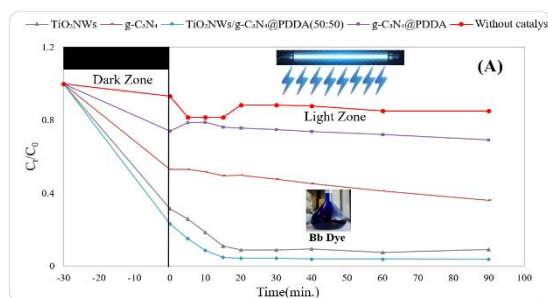Fig.6. (A) Cationic polyelectrolyte (PDDA), (B) basic blue cationic dye.

Fig.7A. The effect of three (g-C$_3$N$_4$, PDDA, and TiO$_2$NWs) components on Basic blue

The effect of TiO$_2$NWs:(PDDA$_{(0.5)}$@g-C$_3$N$_4$) percentage on Bb degradation

To determine the effect of the PDDA$_{(0.5)}$@g-C$_3$N$_4$ percentage on photocatalytic performance, the role of the PDDA$_{(0.5)}$@g-C$_3$N$_4$ percentage is

investigated. The PDDA$_{(0.5)}$ @ g-C$_3$N$_4$ content is varied from 30% to 70% (the percentages denoting the weight percentages of the TiO$_2$NWs to (PDDA$_{(0.5)}$ @ g-C$_3$N$_4$). The photocatalytic performance of the prepared nanocomposite with (50:50)% and (30:70)% TiO$_2$NWs/(PDDA$_{(0.5)}$@g-C$_3$N$_4$ is 96% and 94%, respectively, of Basic blue (**Fig. 7B**).Among the prepared catalysts, the catalyst with (50:50) of TiO$_2$NWs/(PDDA$_{(0.5)}$ @ g-C$_3$N$_4$) exhibited the highest photocatalytic activity, while (70:30) of TiO$_2$NWs/(PDDA$_{(0.5)}$ @ g-C$_3$N$_4$) exhibited the lowest photocatalytic activity (92%), based on the Bb degradation efficiency.
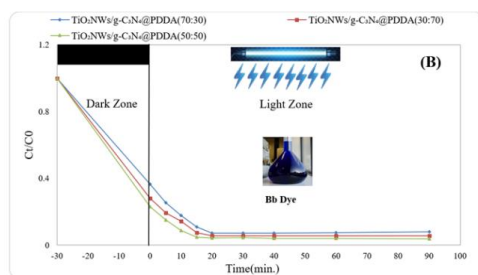

Fig.7B. The effect of TiO$_2$NWs:(PDDA$_{(0.5)}$ @ g-C$_3$N$_4$) percentage on Bb degradation

3.5.2. Effect of PDDA concentrations

The effect of modified catalysts with PDDA on basic blue degradation was studied using TiO$_2$NWs/(PDDA$_{(0.5)}$@g-C$_3$N$_4$)with different PDDA concentrations (0.1, 0.5, and 1.0 wt.%) compared to the unmodified catalyst (TiO$_2$NWs/g-C$_3$N$_4$) (**Fig. 7C**).It is observed that the adsorption capability of the catalysts after PDDA modification has an obvious improvement owing to the positive charge effect on the surfaces of the PDDA $_{(0.5)}$@g-C$_3$N$_4$ where PDDA acts as an effective binder to negatively charged TiO$_2$NWs on the surface of g-C$_3$N$_4$. PDDA is a positively charged branched polymer that can be adsorbed onto the surface of g-C$_3$N$_4$ via electrostatic interactions, thereby changing the surface of g-C$_3$N$_4$ from negatively charged to positively charged [62], thereby establishing layers of PDDA$_{(0.5)}$@g-C$_3$N$_4$, TiO$_2$NWs, and PDDA$_{(0.5)}$@g-C$_3$N$_4$, which prevents restacking of g-C$_3$N$_4$ nanosheet the synthesized photocatalysts show high activity and stability [63] because PDDA acts as an electron withdrawal and thus inhibits the recombination of generated electrons [64, 65]. The degradation efficiency of nanocomposite with PDDA concentration (0.1, 0.5, and 1.0 wt.%) is 94%, 96%, and 91%, respectively. However, the concentration of PDDA solution above 0.5 wt% would have an adverse effect on the degradation efficiency of nanocomposite, where the degradation efficiency is 79.6% for unmodified catalyst (TiO$_2$NWs/g-C$_3$N$_4$).
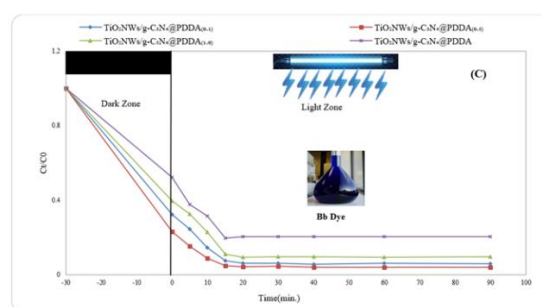

Fig.7C. Effect of PDDA concentrations

3.5.3. The Effect of dye concentration

An experiment was carried out to examine the influence of initial Methylene blue concentration on the photocatalytic activity of TiO$_2$NWs/(PDDA$_{(0.5)}$@g-C$_3$N$_4$)nanocomposite. The experiment was carried out by adding 1 g/L of catalysts to the different initial Bb concentrations of 5, 10, and 20 ppm, keeping the dye solution at pH 7. Degradation efficiency for different initial dyes is shown in **Fig. 7D**. The maximum degradation was obtained at 5 ppm, but we chose 10 ppm for all degradation processes. The rate of the photogdegradation of Bb dye depends on the eventuality of the formation of an OH* radical on the surface of the catalyst and the reaction of dye molecules with the OH* radical. The initial promotion in the rate of degradation with an increase in initial Methylene blue dye concentration is shown in Fig. 8D and might be attributed to an increase in the eventuality of the reaction between OH* radical and molecules of dye [66]. Anyway, increasing the concentration of dye (20 ppm) reduces the activity of the catalyst. Where, as more molecules of dye are adsorbed on the surface of the catalyst at a high concentration of dye, thereby decreasing the formation of the OH* radical, which is responsible for the dye degradation [67]. Increasing absorption or scattering of light at high concentrations of the dye molecules in solution also decreases the photons reaching the catalyst surface, thus decreasing the photo-degradation rate of Basic blue [68].
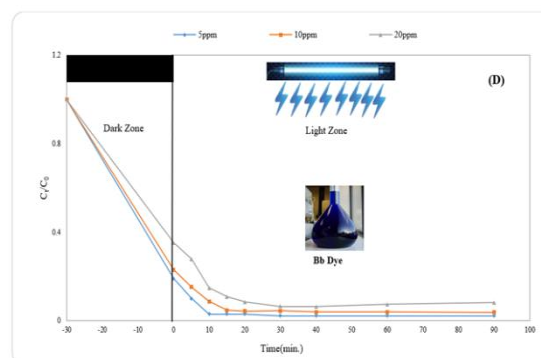

Fig.7D. The Effect of dye concentration

3.5.4. Effect of dye type (cationic, anionic)

To determine the synergistic effects of PDDA $_{(0.5)}$ @ g-C$_3$N$_4$ and TiO$_2$NWs on the photocatalytic degradation of different organic dyes (cationic and anionic), the evaluations of photocatalytic degradation were performed by using Methyl Orange and Basic Blue dyes under UV-Vis light irradiation. As shown in **Fig. 7E**, the adsorption property of the anionic dye, Methyl Orange, can be neglected over the prepared TiO$_2$NWs/(PDDA$_{(0.5)}$@g-C$_3$N$_4$)composites. Due to its limited adsorption within visible light and fast electron-hole pair recombination, pure g-C$_3$N$_4$ has a moderate activity for photodegradation of Methyl Orange under UV-Vis irradiation, with the maximum degradation reaching 80.9% after 10 minutes and gradually decreasing to 68.8% at the end of 120 minutes. However, the photocatalytic activity of the TiO$_2$NWs sample is not clearly higher than pure g-C$_3$N$_4$, where the maximum degradation reached 42.7% after 10 min of irradiation and then decreased gradually to 6.5% at the end of 120 min. On the other hand, the photocatalytic effect was also studied by observation of the degradation of Basic Blue under the same conditions as that of Methyl Orange, and the outcome is shown in Fig. 8A. As shown in Fig. 8A, the obtained TiO$_2$NWs/ (PDDA$_{(0.5)}$@g-C$_3$N$_4$)composites display a perfect adsorption tendency toward Basic Blue dye. The adsorption is about 96% of dye molecules within 120 min, while the adsorption of Basic blue in the presence of pure g-C$_3$N$_4$ and TiO$_2$NWs is 63.7% and 90.7%, respectively. The high activity of TiO$_2$NWs/(PDDA$_{(0.5)}$@g-C$_3$N$_4$)composites could be ascribed to the electrostatic interactions between the TiO$_2$NWs/(PDDA$_{(0.5)}$@g-C$_3$N$_4$)composites and cationic Basic blue molecules. From the adsorption tendency of the composites toward anionic dye, it can be deduced that the main factor responsible for the high adsorption ability of the cationic dye is the electrostatic interactions.

The adsorption of dyes depends mainly on the nature of the TiO$_2$NWs/(PDDA$_{(0.5)}$@g-C$_3$N$_4$)composite surface. It is known that the photocatalysis of liquid-solid heterogeneous is a process that is based on the interface [69]. The surface contact between the catalyst and dye molecules is desired for the effective transfer of the generated electrons and active intermediate species such as O$_2$, H$_2$O$_2$, and OH from the TiO$_2$NWs/(PDDA$_{(0.5)}$@g-C$_3$N$_4$)photocatalysts to dyes [70]. It is simply confirmed that the increased dye adsorption contributes to the high activity of the TiO$_2$NWs/(PDDA$_{(0.5)}$@g-C$_3$N$_4$) composite photocatalysis.
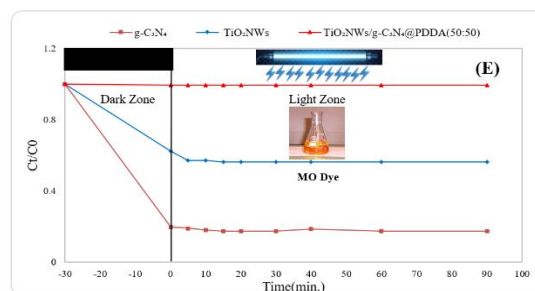

Fig.7E. The Effect of dye type (cationic, anionic)

3.5.5. The Effect of weight of TiO$_2$NWs/(PDDA$_{(5)}$@g-C$_3$N$_4$)nanocomposite

To evaluate the best photocatalyst weight, some degradation processes were performed by varying the weight of the catalyst from 0.5-2g/L at pH 7. The effect of catalyst weight on the degradation rate is shown in **Fig. 7F**. As a result, 1.0 g/L is the optimum catalyst weight for the degradation of basic blue. It is noticed that as catalyst weight increased from 0.5 to 1.0 g/L, the rate of degradation increased. This is due to an increase in the number of absorbed photons and dye molecules. The decrease originated with an increase of more than 1.0 g/L of catalyst weight. This may be attributed to the aggregation of the nanocomposite at high concentrations. This leads to a decrease in the number of active sites that are available at the surface and increases the light scattering at high concentrations of catalyst, leading to a diminishing in the light crossing the catalyst [71].
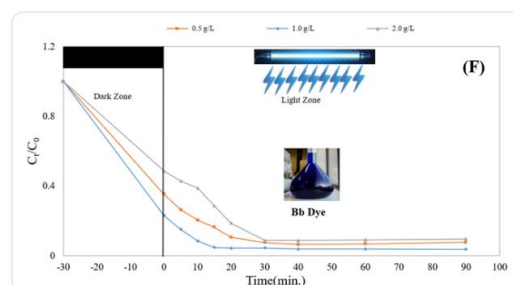

Fig.7F. The Effect of dye type (cationic,

3.6. Photovoltaic performance

The J–V curves were plotted as shown in **Fig.8** to study the effective photovoltaic performance of TiO$_2$NWs, TiO$_2$NWs/(PDDA$_{(0.5)}$@g-C$_3$N$_4$)(50:50) and TiO$_2$NWs/(PDDA $_{(0.5)}$@g-C$_3$N$_4$)(30:70) as photoanodes. The QDSSC of each photoanode was fabricated and tested. The obtained parameters, such as conversion efficiency (CE), fill factor (FF), open circuit voltage (Voc) and current density (Jsc), are summarized in **Table 1.** Superior performance with a conversion efficiency of CE = 1.7 % with Voc = 400 mV and Jsc = 7.84 mA cm^{-2} was obtained for the QDSSC fabricated using TiO$_2$NWs/(PDDA $_{(0.5)}$ @ g-

C_3N_4)(50:50), which is higher compared to the photovoltaic parameter values for pure TiO_2NWs & g-C_3N_4 (30:70), respectively (CE = 1.1 & 1.4%). TiO_2 is a low-cost semiconductor that has the advantages of being non-toxic, harmless, and easy to synthesize [72]. Because of the large bandgap of TiO_2, it can absorb ultraviolet range. In addition, photo-reduced electrons and holes possess high

reducing and oxidizing properties. g-C_3N_4 possessed a special graphite-like electronic band structure with thermal and chemical stability. In comparison to graphene, g-C_3N_4 can be easily obtained using low-cost methods [73]. Combining g-C_3N_4 with other materials could improve the visible light absorption capacity. Therefore, g-C_3N_4 is expected to enhance composite photocatalytic activity.

Table (1) study the effective QDSSCs performance for different working electrode

Working electrode	Voc, (mV)	Jsc, (mA/cm²)	Ppp, (mw/cm²)	FF	CE %
TiO₂NWs	340	6.67	1.1	0.49	1.1
(50:50)	400	7.84	1.74	0.55	1.7
(30:70)	370	7.25	1.42	0.52	1.4
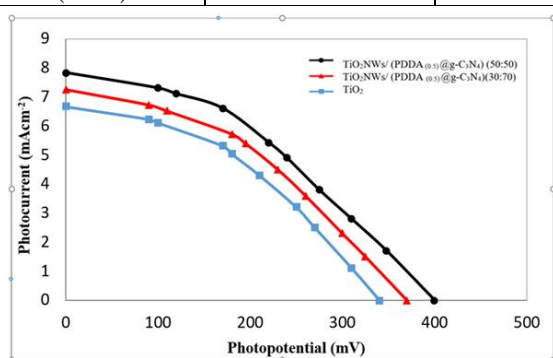
Fig.8. The J-V curves of, TiO_2NWs/(PDDA $_{(0.5)}$@g-C_3N_4)(50:50), TiO_2NWs/(PDDA $_{(0.5)}$@g-C_3N_4)(30:70) and TiO_2NWs

3.7. Effect of QD layers on QDSSCs' performance

The effect of QD layers was studied using the most promising cell in the previous section (20 µm thicknesses of TiO_2NWs/(PDDA$_{(0.5)}$@g-C_3N_4)(50:50) as the working electrode, polysulfide electrolyte, and 20 µm thickness of g-C_3N_4 as the counter electrode). The effect of CdS QDs on the produced electrical

output was reported in **Table 2** and **Fig. 9.** The results show that as the quantum dot layers increase, the open circuit potential, fill factor, and current density increase, and maximum cell efficiency was achieved at 7 cycles of CdS QDs (2.8%).
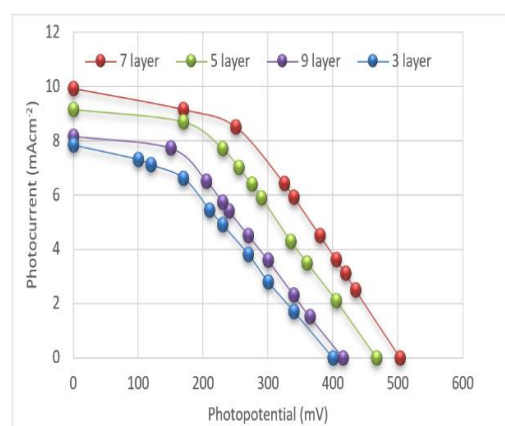

Fig.9. Effect of QD layers on QDSSCs'

Table (2) Effect of CdS QDs layer and the electrical output

CdS QDs layer	Voc, (mV)	Jsc, (mA/cm²)	Ppp, (mw/cm²)	FF	CE %
3	400	7.84	1.74	0.55	1.7
5	467	9.16	2.4	0.56	2.3
7	504	9.92	2.99	0.58	2.8
9	416	8.16	1.86	0.55	1.9

4. Conclusion

TiO_2NWs/ (PDDA $_{(0.5)}$ @g-C_3N_4) nanocomposite was successfully synthesize by the wet impregnation method. The characterization of the synthesized nanocomposite was carried out via XRD, FT-IR, HRTEM, SEM, EDS, mapping, and XPS. Highly adsorption-photodegradation capacity for basic blue dye over microwave-assisted sol-gel anatase TiO_2 nanowire decorated with PDDA $_{(0.5)}$ @ g-C_3N_4 nanosheet under UV-Vis light irradiation as compared to pure TiO_2NWs and PDDA $_{(0.5)}$ @ g-C_3N_4 nanosheets. The photovoltaic performance is

better than the photovoltaic values for pure TiO_2NWs and TiO_2NWs/(PDDA$_{(0.5)}$@g-C_3N_4)(30:70) ,respectively. From this study, we can conclude that TiO_2NWs/(PDDA $_{(0.5)}$ @g-C_3N_4)can be used as a promising tool for solar cell applications in addition to its adsorption-photodegradation properties.

5. Conflicts of interest

The authors declare that they have no conflict of interest.

7. References

[1] S. Tian, Z. Wang, W. Gong, W. Chen, Q. Feng, Q. Xu, C. Chen, C. Chen, Q. Peng, L. Gu, H. Zhao, P. Hu, D. Wang, Y. Li, Temperature-controlled selectivity of hydrogenation and hydrodeoxygenation in the conversion of biomass molecule by the Ru1/mpg-C_3N_4 catalyst, J. Am. Chem. Soc. 140 (2018) 11161-11164.

[2] H. Liu, X. Liu, W. Yang, M. Shen, S. Geng, C. Yu, B. Shen, Y. Yu, Photocatalytic dehydrogenation of formic acid promoted by a superior PdAg@g-C_3N_4 Mott-Schottky heterojunction, J. Mater. Chem. A 7 (2019) 2022-2026.

[3] M. Mousavi, A. Habibi-Yangjeh, S.R. Pouran, Review on magnetically separable graphitic carbon nitride-based nanocomposites as promising visible-light-driven photocatalysts, J. Mater. Sci: Mater. Electron. 29 (2018) 1719-1747.

[4] M. Pirhashemi, A. Habibi-Yangjeh, S.R. Pouran, Review on the criteria anticipated for the fabrication of highly efficient ZnO-based visible-light-driven photocatalysts, J. Ind. Eng. Chem. 62 (2018) 1-25.

[5] M. Shekofteh-Gohari, A. Habibi-Yangjeh, M. Abitorabi, A. Rouhi, Magnetically separable nanocomposites based on ZnO and their applications in photocatalytic processes: A review, Crit. Rev. Env. Sci. Tec. 48 (2018) 806-857.

[6] W. Niu, K. Marcus, L. Zhou, Z. Li, L. Shi, K. Liang, Y. Yang, Enhancing electron transfer and electrocatalytic activity on crystalline carbon-conjugated g-C_3N_4, ACS Catal. 8 (2018) 1926-1931.

[7] Q. Chen, H. Hou, D. Zhang, S. Hu, T. Min, B. Liu, C. Yang, W. Pu, J. Hu, J. Yang, Enhanced visible-light driven photocatalytic activity of hybrid ZnO/g-C_3N_4 by high performance ball milling, J. Photoch. Photobio. A 350 (2018) 1-9.

[8] J. Ran, W. Guo, H. Wang, B. Zhu, J. Yu, S.Z. Qiao, Metal-free 2D/2D phosphorene/g-C_3N_4 vander waals heterojunction for highly enhanced visible-light photocatalytic H_2 production, Adv.Mater. 30 (2018) 1800128.

[9] Q. Xu, B. Cheng, J. Yu, G. Liu, Making co-condensed amorphous carbon/g-C_3N_4 composites with improved visible-light photocatalytic H_2-production performance using Pt as cocatalyst, Carbon 118 (2017) 241-249.

[10] J. Wang, Z. Yang, X. Gao, W. Yao, W. Wei, X. Chen, R. Zong, Y. Zhu, Core-shell g-C_3N_4@ ZnO composites as photoanodes with double synergistic effects for enhanced visible-light photoelectrocatalytic activities, Appl. Catal. B 217 (2017) 169-180.

[11] H. Yu, L. Shang, T. Bian, R. Shi, G.I.N. Waterhouse, Y. Zhao, C. Zhou, L.Z. Wu, C.H. Tung, T. Zhang, Nitrogen-doped porous carbon nanosheets templated from g-C_3N_4 as metal-free electrocatalysts for efficient oxygen reduction reaction, Adv. Mater. 28 (2016) 5080-5086.

[12] G. Xu, H. Zhang, J. Wei, H.X. Zhang, X. Wu, Y. Li, C. Li, J. Zhang, J. Ye, Integrating the g-C_3N_4 nanosheet with B-H bonding decorated metal-organic framework for CO_2 activation and photoreduction, ACS Nano 12 (2018) 5333-5340.

[13] H. Li, F. Li, Z. Wang, Y. Jiao, Y. Liu, P. Wang, X. Zhang, X. Qin, Y. Dai, B. Huang, Fabrication of carbon bridged g-C_3N_4 through supramolecular self-assembly for enhanced photocatalytic hydrogen evolution, Appl. Catal. B 229 (2018) 114-120.

[14] G. Ge, X. Guo, C. Song, Z. Zhao, Reconstructing supramolecular aggregates to nitrogen-deficient g-C_3N_4 bunchy tubes with enhanced photocatalysis for H_2 production, ACS Appl. Mater. Interfaces 10 (2018) 18746-18753.

[15] Q.T.H. Ta, G.Namgung, J.S. Noh, Facile synthesis of porous metal-doped ZnO/g-C_3N_4 composites for highly efficient photocatalysts, J. Photoch. Photobio. A 368 (2019) 110-119.

[16] M. Zhang, C. Lai, B. Li, D. Huang, G. Zeng, P. Xu, L. Qin, S. Liu, X. Liu, H. Yi, M. Li, C. Chu and Z. Chen, Rational design 2D/2D BiOBr/CDs/g-C_3N_4 Z-scheme heterojunction photocatalyst with carbon dots as solid-state electron mediators for enhanced visible and NIR photocatalytic activity: Kinetics, intermediates, and mechanism insight, J. Catal. 369 (2019) 469-481.

[17] K. He, J. Xie, Z.Q. Liu, N. Li, X. Chen, J. Huf, X. Li, Multi-functional Ni_3C cocatalyst/g-C_3N_4 nanoheterojunctions for robust photocatalytic H_2 evolution under visible light, J. Mater. Chem. A 6 (2018) 13448-13122.

[18] C. Liu, Y. Qiu, J. Zhang, Q. Liang, N. Mitsuzaki, Z. Chen, Construction of CdS quantum dots modified g-C_3N_4/ZnO heterostructured photoanode for efficient photoelectrochemical water splitting, J. Photoche. Photobio. A 371 (2019) 109-117.

[19] Z. Lu, L. Zeng, W.L. Song, Z.Y. Qin, D.W. Zeng, C.S. Xie, Appl. Catal. B: Environ. 202 (2017) 489.

[20] Abd-Ellatif, W.R., Mahmoud, N.G., Hashem, A.A., El-Aiashy, M.K., Ezzo, E.M., Mahmoud, S.A., 2022. Efficient photodegradation of E124 dye using two-dimensional Zn-Co LDH: kinetic and thermodynamic studies. Environ. Technol. Innovat. 27, 102393.

[21] X.W. Shi, M. Fujitsuka, Z.Z. Lou, P. Zhang, T. Majima, J. Mater. Chem. A 5 (2017) 9671.

[22] H.L. Li, Y. Gao, X.Y. Wu, P.H. Lee, K. Shih, Appl. Surf. Sci. 402 (2017) 198.

[23] G.Y. Li, X. Nie, J.Y. Chen, Q. Jiang, T.C. An, P.K. Wong, H.M. Zhang, H.J. Zhao, H.Yamashita, Water Res. 86 (2015) 17.

[24] X.-j. Wang, W.-y. Yang, F.-t. Li, Y.-b. Xue, R.-h. Liu, Y.-j. Hao, In situ microwave-assisted synthesis of porous N-TiO_2/g-C_3N_4 heterojunctions with enhanced visible-light photocatalytic properties, Ind. Eng. Chem. Res., 52 (2013) 17140-17150.

[25] X. Chen, J. Wei, R. Hou, Y. Liang, Z. Xie, Y. Zhu, X. Zhang, H. Wang, Appl. Catal. B: Environ. 188 (2016) 342-350.

[26] C. Liu, L. Zhang, R. Liu, Z. Gao, X. Yang, Z. Tu, F. Yang, Z. Ye, L. Cui, C. Xu, Y. Li, J. Alloys Compd. 656 (2016) 24-32.

[27] Shah, S.I., Mahmoud, S.A., Bendary, S.H. et al. Efficient removal of 2-chlorophenol from aqueous solution using TiO$_2$ thin films/alumina disc as photocatalyst by pulsed laser deposition. Appl Water Sci 11, 44 (2021).

[28] MA Betiha, SA Mahmoud, MF Menoufy, AM Al-Sabagh, One-pot template synthesis of Ti–Al-containing mesoporous silicas and their application as potential photocatalytic degradation of chlorophenols, Applied Catalysis B: Environmental, 2011, , 107, 3–4, 316-326.

[29] RA Elsalamony, SA Mahmoud, Preparation of nanostructured ruthenium doped titania for the photocatalytic degradation of 2-chlorophenol under visible light, - Arabian Journal of Chemistry, 10, 2, 2017, 194-205.

[30] SA Mahmoud, E Yassitepe, SI Shah - Materials Science Forum, Photolysis and photocatalysis of 1, 4 dichlorobenzene using sputtered TiO$_2$ thin films, 734, 2013, 215-225.

[31] Tamer E. Emam, Eglal R. Souaya, M. B. M. Ibrahim & Sawsan A. Mahmoud (2022) Advanced removal of pesticides, herbicides, and pharmaceutical residues from surface water, Environmental Technology.

[32] Y. Sang, Z. Zhao, J. Tian, P. Hao, H. Jiang, H. Liu, J.P. Claverie, Small 10 (2014) 3775-3782.

[33] N. Liu, V. Häublein, X. Zhou, U. Venkatesan, M. Hartmann, M. Mačković, T. Nakajima, E. Spiecker, A. Osvet, L. Frey, P. Schmuki, Nano Lett. 15 (2015) 6815-6820.

[34] X. Pan, Y. Zhao, S. Liu, C.L. Korzeniewski, S. Wang, Z. Fan, ACS Appl. Mater Interfaces 4 (2012) 3944-3950.

[35] Q. Xiang, B. Cheng, J. Yu, Appl. Catal. B: Environ. 138–139 (2013) 299-303.

[36] Y. Xue, X. Wang, Int. J. Hydrogen Energy 40 (2015) 5878-5888.

[37] L. Chen, X. Zhou, B. Jin, J. Luo, X. Xu, L. Zhang, Y. Hong, Int. J. Hydrogen Energy 41(2016) 7292-7300.

[38] Matthew A. Hood, Margherita Mari and Rafael Muñoz-Espí, Synthetic Strategies in the Preparation of Polymer/Inorganic Hybrid Nanoparticles, Materials 2014, 7, 4057-4087.

[39] Y. Wang, S. Zhang, D. Du, Y.Y. Shao, Z.H. Li, J. Wang, M. Engelhard, J.H. Li and Y.H. Lin, J. Mater. Chem. 21 (2011) 5319-5325.

[40] S. Zhang, Y.Y. Shao, H.G. Liao, M.H. Engelhard, G.P. Yin, Y.H. Lin, ACS Nano 5 (2011) 1785-1791.

[41] Shojaei AF, Loghmani MH (2012) Effect of microwave irradiation on morphology and size of anatase nano powder: Efficient photodegradation of 4-nitrophenol by W-doped Titania. Bulletin of the Korean Chemical Society 33 (12):3981-3986.

[42] Asiah M. N., Mohd F. A., Mohamad H. M., Musa M. Z., Saifollah A. and Mohamad R. M., (2012) Synthesis of TiO$_2$ Nanowires via Hydrothermal Method. Japanese Journal of Applied Physics 51(06FG08).

[43] Jinghai Liu, Tiekai Zhang, Zhichao Wang, Graham Dawson and Wei Chen, Simple pyrolysis of urea into graphitic carbon nitride with recyclable adsorption and photocatalytic activity, J. Mater. Chem., 2011,21, 14398-14401.

[44] Xin Wang, Xuejiang Wang, Jianfu Zhao, Jingke Song, Chenliang Su, Zhongchang Wang, Surface modified TiO$_2$ floating photocatalyst with PDDA for efficient adsorption and photocatalytic inactivation of Microcystis aeruginosa, Water Research, 2018,131, 320-333.

[45] C. Miranda, H. Mansilla, J. Yáñez, S. Obregón, G. Colón, Improved photocatalytic activity of g-C$_3$N$_4$/TiO$_2$ composites prepared by a simple impregnation method, J. Photochem. Photobiol. A 253 (2013) 16–21.

[46] T Tyborski, C Merschjann, S Orthmann, F Yang, M-Ch Lux-Steiner and The Schedel-Niedrig, Crystal structure of polymeric carbon nitride and the determination of its process-temperature-induced modifications, Journal of Physics,25(2013) 395402.

[47] Y.J. Zhang, A. Thomas, M. Antonietti, X.C. Wang, Journal of the American Chemical Society 131 (2009) 50–51.

[48] Y.J. Wang, R. Shi, J. Lin, Y.F. Zhu, Energy & Environmental Science 4 (2011) 2922–2929.

[49] J. Wang, W.D. Zhang, Electrochimica Acta 71 (2012) 10–16.

[50] S.C. Yan, Z.S. Li, Z.G. Zou, Langmuir 25 (2009) 10397–10401.

[51] X. Yu, Z.H. Li, J.W. Liu, P.G. Hu, Appl. Catal. B: Environ. 205 (2017) 271.

[52] Song, J.; Wang, X.; Ma, J.; Wang, X.; Wang, J.; Xia, S.; Zhao, J. Removal of Microcystis aeruginosa and Microcystin-LR using a graphitic-C$_3$N$_4$/TiO$_2$ floating photocatalyst under visible light irradiation. Chem. Eng. J. 2018, 348, 380-388.

[53] Song J, Wang X, Ma J, Wang X, Wang J, Xia S, Zhao J (2018) Removal of Microcystis aeruginosa and Microcystin-LR using a graphitic-C$_3$N$_4$/TiO$_2$ floating photocatalyst under visible light irradiation. Chem Eng J 348:380–388.

[54] X. Lu, Q. Wang, D. Cui, Preparation and photocatalytic properties of g-C$_3$N$_4$/TiO$_2$ hybrid composite, J Mater. Sci. Technol., 26 (2010) 925-930.

[55] K. Li, Z. Huang, X. Zeng, B. Huang, S. Gao, J. Lu, Synergetic Effect of Ti^{3+} and Oxygen Doping on Enhancing Photoelectrochemical and Photocatalytic Properties of TiO$_2$/g-C$_3$N$_4$ Heterojunctions, ACS Appl. Mater. Interfaces, 9 (2017), 11577-11586.

[56] H. Al-Kandari, A. M. Abdullah, Yahia H. Ahmad, S. Al-Kandari, Siham Y. AlQaradawi, A. M. Mohamed. An efficient eco advanced oxidation process for phenol mineralization using a 2D/3D nanocomposite photocatalyst and visible light irradiations. Sci. Rep. 2017, 7,9898.

[57] Qian Zhang, Yihe Zhang, Zilin Meng, Wangshu Tong, Xuelian Yu, Qi An, Constructing the magnetic bifunctional graphene/titania nanosheet-based composite photocatalysts for enhanced visible-light photodegradation of MB and electrochemical ORR from polluted water, Scientific Reports, 2017, 7: 12296.

[58] Feng C, Wang S and Geng B, (2011) Ti(iv) doped WO$_3$ nanocuboids: fabrication and enhanced visible-light-driven photocatalytic performance. Nanoscale, 3: 3695-3699.

[59] Sankeerthana Bellamkonda ,G.Ranga Rao,(Nanojunction-mediated visible light photocatalytic enhancement in heterostructured ternary BiOCl/ CdS/g-C$_3$N$_4$ nanocomposites), Catalysis Today, 321–322, 2019, 18-25.

[60] X. Bai, L. Wang, Y. Zhu, ACS Catal. 2012, 2, 2769.

[61] B.Luo, X. Yan, S. Xu, Q. Xue, Electrochim. Acta 2012, 59, 429– 434.

[62] L. Zhang , X. He , X. Xu , C. Liu , Y. Duan , L. Hou , Q. Zhou , C. Ma , X.Yang , R. Liu , F. Yang , L. Cui , C. Xu and Y. Li , Highly active TiO$_2$/g-C$_3$N$_4$/G photocatalyst with extended spectral response towards selective reduction of nitrobenzene, Appl. Catal., B, 2017, 203 , 1-8.

[63] Yang, D. Q.; Rochette, J. F.; Sacher, E. Spectroscopic Evidence for π-π Interaction between Poly(diallyl dimethylammonium) Chloride and Multiwalled Carbon Nanotubes. J Phys. Chem. B 2005, 109, 4481–4484.

[64] Wang, S.; Yu, D.; Dai, L. Polyelectrolyte Functionalized Carbon Nanotubes as Efficient Metal-free Electrocatalysts for Oxygen Reduction. J. Am. Chem. Soc. 2011, 133, 5182–5185.

[65] Akpan UG, Hameed BH (2009) Parameters affecting the photocatalytic degradation of dyes using TiO$_2$-based photocatalysts: a review. Journal of hazardous materials 170 (2-3):520-529.

[66] Jantawasu P, Sreethawong T, Chavadej S (2009) Photocatalytic activity of nanocrystalline mesoporous-assembled TiO$_2$ photocatalyst for degradation of methyl orange monoazo dye in aqueous wastewater. Chemical Engineering Journal 155 (1-2):223-233.

[67] Sahoo C, Gupta AK, Sasidharan Pillai IM (2012) Photocatalytic degradation of methylene blue dye from aqueous solution using silver ion-doped TiO$_2$ and its application to the degradation of real textile wastewater. Journal of Environmental Science and Health, Part A 47 (10):1428-1438.

[68] K. Bourikas, M. Stylidi, D.I. Kondarides, X.E. Verykios, Langmuir 21 (2005) 9222.

[69] Sohrabnezhad, S., Pourahmadee, A., Rada, E., Photocatalytic degradation of basic blue 9 by CoS nanoparticles supported on AlMCM-41 material as a catalyst. J. Hazard. Mate.,170,184-190,2009.

[70] Zhang, X. K.; Li, L.; Zeng, Y. Q.; Liu, F.; Yuan, J. J.; Li, X. K.; Yu, Y.; Zhu, X. R.; Xiong, Z. Z.; Yu, H. J.; Xie, Y. M. TiO2/Graphitic Carbon Nitride Nanosheets for the Photocatalytic Degradation of Rhodamine B under Simulated Sunlight. ACS Appl. Nano Mater. 2019, 2, 7255-7265.

[71] Zhang, M. Y.; Qin, J. Q.; Rajendran, S.; Zhang, X. Y.; Liu, R. Heterostructured d-Ti$_3$C$_2$/TiO$_2$/g-C$_3$N$_4$ nanocomposites with enhanced visible-light photocatalytic hydrogen production activity. ChemSusChem. 2018, 11, 4226-4236.

[72] Monga, D.; Basu, S. Enhanced photocatalytic degradation of industrial dye by g-C$_3$N$_4$/TiO$_2$ nanocomposite: Role of shape of TiO$_2$. Advanced Powder Technology. 2019, 30, 1089-1098.

[73] Hu, C. Y.; E, L.; Hu, K. K.; Lai, L.Y.; Zhao, D.; Zhao, W.; Rong, H. Simple synthesis of 3D flower-like g-C$_3$N$_4$/TiO$_2$ composite microspheres for enhanced visible-light photocatalytic activity. Journal of Materials Science. 2020, 55, 151-162.